Dyed Microspheres for Quantification of UV Dose Distributions: Photochemical Reactor Characterization by Lagrangian Actinometry

Ernest R. Blatchley III[1]; Chengyue Shen[2]; Zorana Naunovic[3]; Lian-Shin Lin[4]; Dennis A. Lyn[5]; J. Paul Robinson[6]; Katherine Ragheb[7]; Gérald Grégori[8]; Donald E. Bergstrom[9]; Shiyue Fang[10]; Yousheng Guan[11]; Kristofer Jennings[12]; and Nilupa Gunaratna[13]

Abstract: Lagrangian actinometry represents a new method of photochemical reactor characterization. The method is based on an application of dyed microspheres, which were developed by attachment of (*E*)-5-[2-(methoxycarbonyl)ethenyl]cytidine (hereafter referred to as *S*) to polystyrene microspheres. *S* is a nonfluorescent molecule that when subjected to ultraviolet (UV) irradiation yields a single product, 3-β-D-ribofuranosyl-2,7-dioxopyrido[2,3-*d*]pyrimidine (hereafter referred to as *P*), which displays a strong fluorescence signal. Dyed microspheres were subjected to UV irradiation under a collimated beam and using a single-lamp, monochromatic (low pressure Hg), continuous-flow reactor. In parallel with these experiments, a biodosimetry experiment was conducted using *Bacillus subtilis* spores as the challenge organism. Particle-specific fluorescence intensity measurements were conducted on samples from the collimated-beam experiments and the flow-through reactor experiments by flow cytometry. Estimates of the dose distribution delivered by the flow-through reactor for each operating condition were developed by deconvolution of data resulting from flow cytometry analysis of these samples. In conjunction with these experiments, a numerical model was developed to simulate the behavior of the reactor system. A commercially available computational fluid dynamics package was used to simulate the flow field, while line-source integration was used to simulate the irradiance field. A particle-tracking algorithm was employed to interrogate the flow and irradiance field simulations for purposes of developing particle-specific (Lagrangian) estimates of dose delivery. Dose distribution estimates from the microspheres assays and the numerical simulations were combined with the measured dose–response behavior of *B. subtilis* spores to yield estimates of spore inactivation in the flow-through experiments. For the range of operating conditions used in these experiments, predictions of spore inactivation based on dose distribution estimates from both methods were in good agreement with each other, and with the measured spore inactivation behavior. Lagrangian actinometry is capable of yielding accurate, detailed measurements of dose delivery by continuous-flow UV systems. This method represents a substantial improvement over existing experiment-based methods of UV reactor characterization (e.g., biodosimetry) in that it yields a measurement of the dose distribution for a given operating condition. This method also represents an improvement over existing methods for validation of numerical simulations. Specifically, because this method yields a measurement of the dose distribution, it is possible to compare these measurements with predicted dose distributions from the numerical simulation. The combined application of biodosimetry, numerical modeling, and Lagrangian actinometry represents an extremely robust approach to reactor characterization and validation.

CE Database subject headings: Dewatering; Reactors; Experimentation.

[1]School of Civil Engineering, Purdue Univ., West Lafayette, IN 47907-2051 (corresponding author). E-mail: blatch@purdue.edu

[2]School of Civil Engineering, Purdue Univ., West Lafayette, IN 47907-2051.

[3]School of Civil Engineering, Purdue Univ., West Lafayette, IN 47907-2051.

[4]School of Civil Engineering, Purdue Univ., West Lafayette, IN 47907-2051.

[5]School of Civil Engineering, Purdue Univ., West Lafayette, IN 47907-2051.

[6]Purdue Univ. Cytometry Laboratories, Purdue Univ., West Lafayette, IN 47907.

[7]Purdue Univ. Cytometry Laboratories, Purdue Univ., West Lafayette, IN 47907.

[8]Purdue Univ. Cytometry Laboratories, Purdue Univ., West Lafayette, IN 47907.

[9]Dept. of Medicinal Chemistry and Molecular Pharmacology, Purdue Univ., West Lafayette, IN 47907 and Walther Cancer Institute, Indianapolis, IN.

[10]Dept. of Medicinal Chemistry and Molecular Pharmacology, Purdue Univ., West Lafayette, IN 47907 and Walther Cancer Institute, Indianapolis, IN.

[11]Dept. of Medicinal Chemistry and Molecular Pharmacology, Purdue Univ., West Lafayette, IN 47907 and Walther Cancer Institute, Indianapolis, IN.

[12]Dept. of Statistics, Purdue Univ., West Lafayette, IN 47907.

[13]Dept. of Statistics, Purdue Univ., West Lafayette, IN 47907.

Introduction

Chemical actinometry is commonly used in photochemistry as an experiment-based (wet chemistry) method for measurement of radiation (Kuhn et al. 1989). Specific applications include measurements of irradiance and dose (fluence) delivery, usually at a fixed location, based on quantifiable, photochemically induced changes to the actinometer. Actinometers that have been used in studies of ultraviolet radiation include: potassium ferrioxalate (Demas et al. 1981; Harris et al. 1987; Hatchard and Parker 1956), potassium peroxodisulphate (Mark et al. 1990a,b), potassium iodide (Rahn 1993, 1997; Rahn et al. 2003), and uridine (Linden and Darby 1997; Zhang et al. 1997).

When subjected to ultraviolet (UV) irradiation, (*E*)-5-[2-(methoxycarbonyl)ethenyl]cytidine (MW 327.3, hereafter referred to as *S*) is transformed to a bright violet fluorescent product, 3-β-D-ribofuranosyl-2,7-dioxopyrido[2,3-*d*]pyrimidine [molecular weight (MW) 295.26, hereafter referred to as *P*]. (Bergstrom et al. 1982; Shen et al. 2005). The phototransformation process is illustrated in Fig. 1. The stable photoproduct, *P*, has a fluorescence excitation maximum at 330 nm and an emission maximum at 385 nm (see Fig. 2). The quantum yield for phototransformation of *S* to *P* in homogeneous aqueous solution has been measured at three germicidally active UV wavelengths, and in all cases was quite high (see Table 1). In the absence of UV radiation, *S* and *P* are extremely stable. Therefore, the reaction of interest is highly efficient as a means of quantitatively transforming a nonfluorescent compound into a fluorescent compound. The efficient generation of a stable, fluorescent photoproduct is unique among actinometers.

The extent of reactant conversion in a photochemical process depends upon the dose of radiation delivered to the photochemical target (parent compound). For continuous-flow, UV-based photochemical reactor systems used in the treatment of fluids, dose delivery is complicated by the existence of strong gradients in the irradiance field and the turbulence characteristics of the flow field. Collectively, these attributes of the system dictate that a *dose distribution* is delivered by the system. The dose distribution and the intrinsic kinetics of the photochemical reaction(s) of interest govern overall reactor performance in photochemical reactor systems (Chiu et al. 1999).

Previously, the only methods available to estimate the UV dose distribution involved numerical simulations of process behavior, usually involving a component approach. The irradiance field may be simulated using one of several available models (e.g., Blatchley 1997). Computational fluid dynamics (CFD) are commonly used to represent the flow field, including its turbulence characteristics (Chiu et al. 1999; Lyn and Blatchley 2005; Lyn et al. 1999). The results of these simulations are integrated to provide a representation of the dose distribution. Most such simulations have followed a Lagrangian approach, in which a particle-tracking algorithm is used to interrogate the simulated flow field. Although Lagrangian simulations are less computationally efficient than comparable Eulerian models, they have the advantage of being relatively easy to describe because of their similarity to the true physical situation being modeled. Moreover, in a Lagrangian modeling approach, estimation of the dose distribution is a natural outcome. It should be noted that dose distribution estimates may also be developed by Eulerian methods; however, most Eulerian models are developed for purposes of predicting reactor performance, and therefore the intermediate step of predicting a dose distribution is usually skipped.

In Lagrangian methods, dose increments are calculated for each particle step within its simulated trajectory, such that an estimate of particle-specific dose can be assigned to each simulated particle trajectory by summation of dose increments. By repeating this process for a large population of particles, it is possible to close on a stable dose distribution estimate.

Although numerical simulations represent powerful tools for characterization of reactor dynamics, they must be validated. Ideally, each component of the model would be validated independently, using separate physical measurements. Unfortunately, it is not possible to apply an actinometer in a homogeneous solution to meet this objective for validation of a dose distribution estimate. Homogeneous actinometers can only be used to provide measurements of local irradiance or local dose delivery. Therefore, the development of an experiment-based method for measurement of the dose distribution delivered by a photochemical reactor represents a potentially important advance.

Methods

Lagrangian Actinometry

It was hypothesized that by imposing a large number of appropriately labeled particles on a system, with downstream sample collection and subsequent measurement of photoproduct formation on each particle, it would be possible to develop an estimate of the dose distribution, based on a Lagrangian frame of reference. *S* was chosen as the dye for use in these experiments because of the characteristics described above.
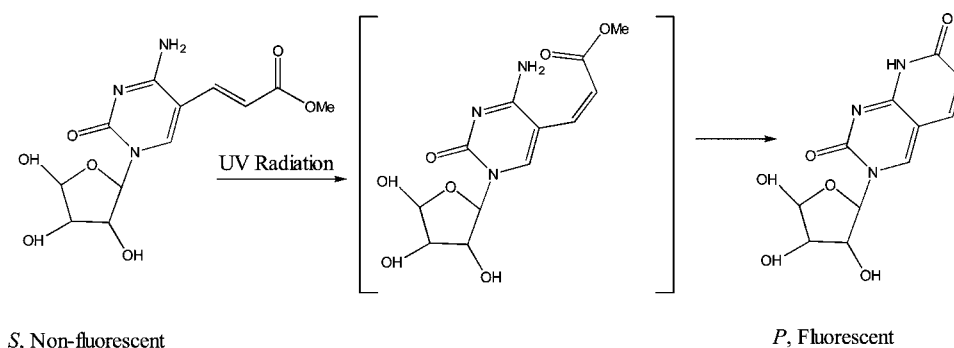

Fig. 1. Basic UV photochemistry of *S* in aqueous solution (adapted from Bergstrom et al. 1982)
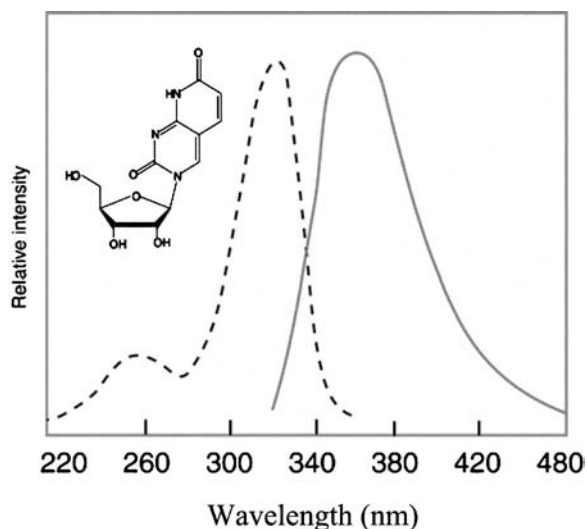
Fig. 2. Fluorescence excitation (dashed) and emission (solid) spectra of P in aqueous solution (Bergstrom et al. 1982)

Fig. 3. Schematic illustration of experimental setup

A critical step in the development of this system was identification of an appropriate method of dye attachment. To be of value in this application, it was necessary to attach S to the microspheres in such a way that the basic photochemistry of interest was not adversely affected, and the fluorescence signal of the photoproduct (P) was not quenched. These objectives were met by S (and P) attachment to microspheres through a streptavidin–biotin linkage using a long hydrophilic linker. The linker favored biotin–streptavidin bonding, and was beneficial in creating microspheres with surface characteristics that did not favor agglomeration, both of which were beneficial in this application (Fang et al. 2003).

Several experiments were conducted to define the fundamental characteristics of the dyed microspheres. The most basic experiment involved UV_{254} irradiation of an aqueous suspension of the dyed microspheres in a well-mixed, shallow, batch reactor under a monochromatic ($\lambda = 254$ nm) collimated beam. The experiment was repeated over a range of UV doses that are relevant to treatment applications. Fluorescence intensity (FI) was measured on the irradiated suspensions using a Cary Eclipse Fluorescence Spectrophotometer (Varian Inc., Walnut Creek, Calif.). Because FI is measured in arbitrary units, the settings for the instrument were fixed to facilitate comparisons between samples. Excitation and emission settings were set to 330 and 385 nm, respectively.

A similar experiment was conducted in which particle-specific FI measurements were conducted by flow cytometry. Samples were analyzed on a Beckman-Coulter Altra sorter, with a data rate of approximately 150–200 particles/s; roughly 15,000 events (particles) were analyzed per sample. Microspheres were excited with the 351 nm line of a 60 mW Coherent Enterprise laser; a linear
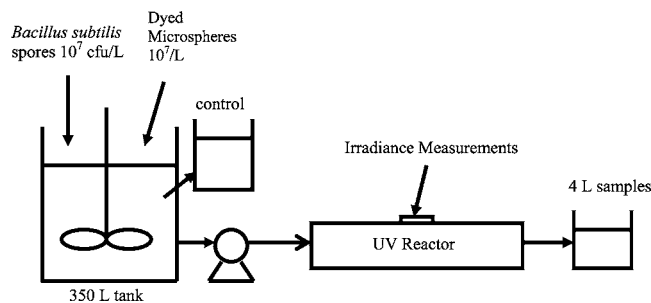
fluorescence signal was measured at 380 nm. Both forward angle light scatter (size related) and orthogonal light scatter (shape and structure related) data were collected.

The characteristic wavelength ($\lambda = 351$ nm) of the laser used with the flow cytometer for these experiments falls within the range of UV wavelengths that will excite P; however, excitation at 351 nm is not as efficient as at $\lambda = 330$ nm (see Fig. 2). Therefore, it may be possible to improve the signal for this measurement by using a laser with a characteristic output that more closely matches the excitation characteristics of P. No such laser was available for use in this research.

Analysis of dyed microspheres by flow cytometry required sample preparation to achieve an appropriate concentration of the microspheres. For each exposure condition, microspheres from a 400-mL sample were separated from the sample by membrane filtration, followed by resuspension in an aqueous buffer, and centrifugation to yield a final (preconcentrated) sample volume of roughly 800 μL. Microsphere recovery by these methods was shown to be approximately 94%. Analysis of preconcentrated samples by flow cytometry was completed in 1–2 min/sample.

The same aqueous suspension of dyed microspheres was pumped through a single-lamp, continuous-flow UV reactor system. The cylindrical reactor walls and the single cylindrical lamp/jacket assembly bounded an annular irradiated zone. The stainless steel wall of the reactor had an internal diameter of 9.55 cm and a length of 75.5 cm. The lamp/jacket assembly had an external diameter of 2.54 cm and spanned the entire length of the irradiated zone. A schematic illustration of the experimental setup is presented in Fig. 3. Experiments were conducted with water from an in-house reverse osmosis system as the base matrix. Dyed microspheres and *Bacillus subtilis* spores (see biodosimetry discussion below) were added to yield concentrations of 10^7 particles/L, each. The resulting aqueous suspension had a transmittance ($\lambda = 254$ nm; 1.0-cm path length) of 99.4%. Untreated water with this composition was used to fill a 350-L influent reservoir. Prior to initiation of experiments, the contents of the influent reservoir were mixed using an impeller system. All experiments were conducted under conditions of dim lighting that allowed instrument readings to be taken, while minimizing expo-

Table 1. Estimates of Quantum Yield for Photoproduction of P from S (from Shen et al. 2005)

λ (nm)	Φ_λ (mole/E) (mean±standard deviation)
222	0.693±0.037
254	0.732±0.064
282	0.850±0.049

Table 2. Volumetric Flow Rates (Q) and Corresponding Mean Hydraulic Detention Times (θ) Used in Experiments with Continuous Flow Reactor

Q (L/s)	$\theta = V/Q$ (s)
0.95	5.29
0.76	6.61
0.57	8.82
0.28	17.9

sure to ambient UV radiation. Experiments were conducted over a range of flow rates that fell within manufacturer recommendations; Table 2 provides a summary of flow rates used in these experiments, as well as the corresponding mean hydraulic detention time at each flow rate.

Before the UV lamp was ignited, the submersible pump in the influent reservoir was started and the gate valve on the feed line was left open so as to obtain the maximum flow rate. A blank sample was collected at the effluent end of the reactor under this condition, after the reactor had been completely purged and steady-state conditions had been achieved. A control sample was also collected directly from the influent reservoir. The pump was then turned off and the lamp was ignited while the reactor remained filled with the aqueous suspension of microspheres and spores. Lamp output was monitored by placing a 31-cm flat-plate collimator against the wall of the reactor so that the axis of the collimator was aimed at the central axis of the lamp, through the quartz viewing window on the side of the reactor. The planar detector of a radiometer (International Light, Newburyport, R.I.) was positioned at the end of the collimator to collect irradiance readings. Lamp output stabilized after approximately three minutes. After achieving a stable lamp output, flow through the reactor was again initiated by turning on the submersible pump. An effluent sample (4 L) was collected at each stable flow rate after at least five reactor volumes had passed through the reactor system. This method of reactor sampling was used to promote steady-state conditions at the time of effluent sample collection. Subsamples were subjected to the preconcentration and flow cytometry procedures described above.

Values of UV irradiance (at the end of the collimator) and volumetric flow rate were monitored throughout the period required to collect each effluent sample. Measured values of these parameters varied by no more than a few percent in each experiment. Values of UV irradiance and volumetric flow rate associated with each experiment (for modeling purposes) were the mean of each value observed during the course of sample collection. After sample collection, the flow rate through the reactor was adjusted with the gate valve. The process was repeated for a range of flow rates that were relevant to the reactor system. Throughout all experiments, water in the influent reservoir was sufficiently deep to prevent pump cavitation.

Detailed measurements of the geometry of the reactor and collimator, as well as the optical characteristics of the system (transmittance and thickness of quartz jacket around lamp, transmittance of aqueous suspension in reactor, transmittance, and thickness of quartz viewing window) were performed. These data were combined with measurements of irradiance (based on collimated radiation, as described above) for estimation of lamp output power by inverse-line-source integration (LSI) modeling (Blatchley 1997). Lamp output power estimates by this method ranged from 13.3 to 13.6 W.

Biodosimetry

Biodosimetry represents a standard method for testing and validation of UV disinfection systems. In this application, the motivation for conducting a microbial challenge was to develop process performance data that could be used to compare with data collected by Lagrangian actinometry and predictions of the Lagrangian numerical model. *Bacillus subtilis* spores were used as the challenge organism in these experiments.

Spore Production

Bacillus subtilis cells (ATCC 6633) were propagated by incubation on nutrient agar plates at 30°C for 24 h. The bacteria were then incubated for 6 days at 35°C on Schaeffer's sporulation agar plates (Schaeffer et al. 1965). After 6 days, spores were harvested and resuspended in sterile nanopure water. Purification of spores was performed following recommended methods (Nicholson et al. 2000). Purity of the spore suspension was examined by optical microscopy using the Schaeffer–Fulton spore stain method (Schaeffer and Fulton 1933).

Dose–Response Experiments

Two different flat-plate collimated beam devices were used to define *Bacillus subtilis* spore inactivation kinetics. A flat-plate collimator with a single low-pressure Hg lamp was used to determine the dose–response behavior for doses up to 50 mJ/cm^2. This collimator produced a highly uniform, nearly monochromatic ($\lambda = 254$ nm) beam of UV radiation at an irradiance of roughly 130 μW/cm^2, and a beam diameter of approximately 6 cm. To deliver higher doses (up to 200 mJ/cm^2) a flat-plate collimator with two mercury amalgam lamps was used, which yielded a nearly monochromatic ($\lambda = 254$ nm), but more powerful beam (incident irradiance of roughly 550 μW/cm^2) than could be accomplished with the smaller collimator. In addition, the larger collimator yielded a larger beam diameter (16 cm), which allowed irradiation of up to 200 mL in a single sample, as compared to 7 mL with the smaller system. For purposes of these experiments, an important feature of this system was that irradiation times required to deliver a given dose were decreased by roughly a factor of four, relative to the smaller collimated beam. Experiments with the two collimated beams included overlapping dose ranges. No difference in spore inactivation was discernable for doses that were common to both collimated beams.

A stock solution of 10^6 viable spores/mL was prepared. For each dose, a subsample of the stock solution was transferred to a Petri dish and exposed to collimated UV radiation for a predetermined period of time to achieve the desired dose. The spore suspension was stirred with a small magnetic stir bar during irradiation to promote a homogeneous distribution of UV radiation. For each UV dose, three different dilutions were each vacuum filtered through a sterile 0.45-μm membrane filter, with the objective of yielding 10–300 colony forming units (cfu) per filter. The lower limit for these analyses (10 cfu) was selected to promote statistical reliability, while the upper limit (300 cfu) was selected to ensure that individual colonies could be discerned. The filters were placed on agar plates and incubated for 24 h at 37°C, followed by colony counting.

Flow-Through Reactor Microbial Challenges

Biodosimetry experiments were conducted in conjunction with Lagrangian actinometry experiments (see Fig. 3). Spores and microspheres (see previous discussion) were added to yield concentrations of 10^7 particles/L, each. Untreated water with the composition described above was used to fill a 350-L influent reservoir.

Because biodosimetry was conducted in conjunction with microsphere challenges, sample collection procedures for quantification of spore viability were identical to those described above for Lagrangian actinometry experiments. Subsamples were subjected to dilution (when necessary), membrane filtration, and plating, as described above.
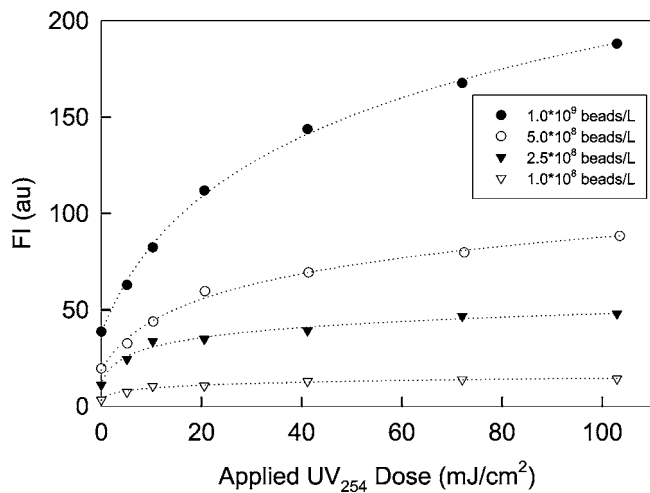
Fig. 4. UV$_{254}$ "dose–response" behavior of dyed microspheres in aqueous suspension. Fluorescence intensity was measured spectrofluorometrically using excitation at 330 nm and emission at 385 nm for range of microsphere concentrations.

Results and Discussion

Measurements of FI for microsphere suspensions by fluorescence spectroscopy are presented in Fig. 4. These data demonstrate several desirable characteristics, including development of a measurable response at UV doses that are relevant in disinfection applications. These data were valuable in that they indicated that the dyed microspheres would provide a fluorescence response that increased monotonically with UV dose and was measurable; however, because spectrofluorometric measurements yield only a single value to characterize an entire population, this method of analysis and the resulting data could not be used to quantify dose distributions. The data in Fig. 4 also illustrate measurable fluorescence character among the nonirradiated microspheres, which is believed to be attributable to the polystyrene microspheres themselves. The FI signal among nonirradiated microspheres was roughly proportional to the concentration of microspheres in suspension. Similar trends in increasing FI as a function of microsphere concentration were also evident for the irradiated microspheres.

Measurement of a dose distribution using dyed microspheres requires that a change in individual microspheres resulting from UV exposure be quantified. Flow cytometry was chosen as the method for measurement of FI at the single particle level among large populations of irradiated microspheres. As configured for this research, the flow cytometer provided extremely sensitive FI measurements for individual microspheres within samples. The sensitivity of flow cytometers is desirable, in that it allows for discrete measurements of the optical characteristics of individual particles among a large population of particles in suspension. However, this sensitivity also introduces a problem in the sense that ambient particles represent a potential source of interference. Ambient particles will always be present in water samples collected from photochemical reactor systems, such as those used in water and wastewater treatment facilities; therefore, steps must be taken to discriminate against these particles in the analysis of dyed microspheres that are introduced for analysis of a UV reactor. The approach used to discriminate against ambient particles is known as "gating."

Gating is a commonly used technique in flow cytometry in

which the known optical characteristics of the particles of interest are used to identify them and differentiate them from ambient particles. For this research, gating was performed on the basis of size (light "blocking") and FI. Gating is a repeatable process that results in substantial simplification of the FI population; more importantly, gating allows the analysis by flow cytometry to focus on the particles of interest only, which in this case were the individual dyed microspheres. Gating was applied to all samples analyzed by flow cytometry in this research. Although gating proved to be a very effective method for elimination of data associated with noise and particles other than the dyed microspheres, it is important to recognize that scatter in FI (i.e., an FI distribution) was evident even in the gated data sets from analysis of samples that had been subjected to the same dose. Therefore, it was necessary to develop a numerical method to extract (deconvolve) the dose distribution from these complex data sets.

The collimated-beam system was used to develop a detailed description of the dose–response behavior of the dyed microspheres. Aqueous microsphere suspensions were subjected to doses ranging from 0 to 200 mJ/cm^2 using this system. This range of doses was selected prior to completion of the numerical simulations of these experiments, and was believed to be representative of the range of doses that would be delivered by the continuous-flow reactor for the range of operating conditions employed in these experiments. Fig. 5 provides a summary of the results of flow cytometry analyses of these samples.

The data in Fig. 5 illustrate a monotonic increase in FI with increasing UV dose, corresponding to photoproduction of *P* from *S*. Although each of the samples from the collimated-beam experiment was subjected to a single-valued dose, the analysis by flow cytometry demonstrated a distribution of FI among the exposed microspheres. Variation in the resulting FI measurements was attributed to intrinsic heterogeneity among the dyed microspheres (size, shape, surface loading of *S*) and errors inherent in FI measurement by flow cytometry.

The data presented in Fig. 5 demonstrate clear trends in the UV dose–response behavior of the dyed microspheres; however, the data in this figure (and others that follow) also include visually evident noise. The noise in these data sets is attributable to the size of the microsphere populations that were analyzed to produce these figures. In particular, each curve in these figures represents a summary (histogram) of the analysis of a population of at least 10,000 particles. This population size was chosen on the basis of Lagrangian numerical simulations of the same reactor system (discussed below) that indicated that a population of 10,000 simulated particle trajectories through the irradiated zone of this reactor system was sufficient to yield a stable dose distribution estimate (i.e., an increase in the population of simulated trajectories above this value did not yield a significant change in the simulated dose distribution). Although noise in Fig. 5 (and related data sets) could have been reduced by increasing the size of the population of microspheres that was analyzed for each exposure condition, this approach was not followed in the research described herein so as to provide consistency between dose distribution estimates developed by Lagrangian actinometry and the Lagrangian numerical model.

Fig. 6 illustrates the results of flow cytometry analysis of samples collected from the continuous-flow reactor experiment. Again, analysis of samples from these experiments demonstrated an FI distribution; however, the distribution was broader than in the collimated-beam experiment. As flow rate increased, the distribution shifted to lower values of FI and became narrower. In qualitative terms, these changes in the FI distribution were en-
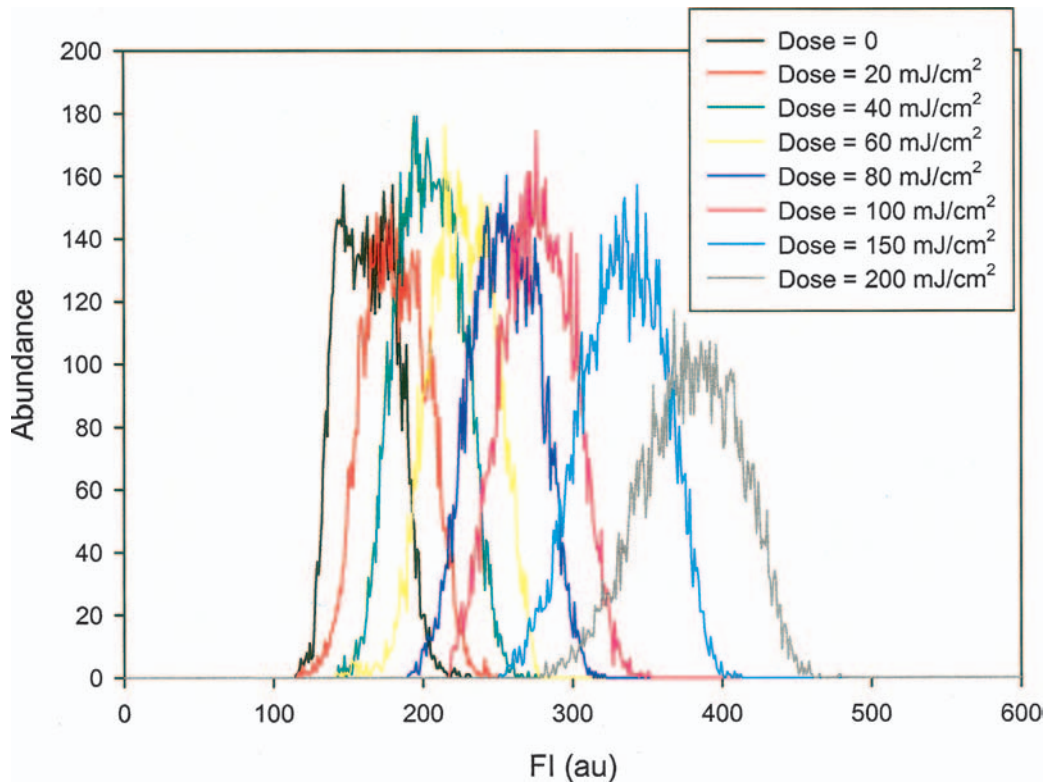
Fig. 5. (Color) Measured FI distributions based on gated populations of dyed microspheres from dose–response (collimated-beam) experiment. These data represent UV_{254} dose–response behavior for dyed microspheres. Distribution in FI was evident in all populations; however, distribution displayed monotonic shift toward higher values of FI as dose increased.
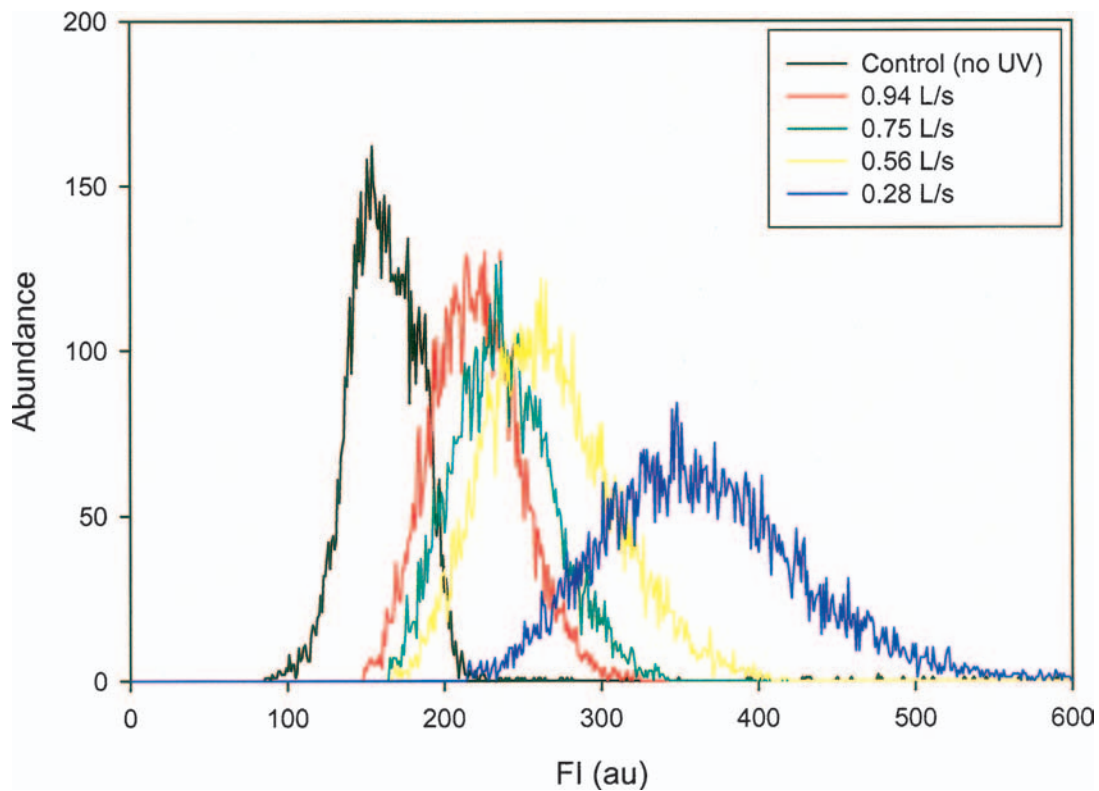

Fig. 6. (Color) Measured FI distributions on gated populations from continuous-flow reactor experiment. Effluent samples were collected from continuous-flow reactor under conditions of steady-state operation at each of flow rates defined in legend.

tirely consistent with the behavior that was expected in this system. Specifically, as flow rate increases, the duration of UV exposure will decrease, and the residence time distribution will become more like a "plug-flow" condition. Collectively, the data presented in Figs. 5 and 6 illustrate characteristics that were consistent with the known behavior of continuous-flow reactor systems.

Convolution Hypothesis and Experiment

Measurements of FI for a "uniform" population of dyed microspheres by flow cytometry will yield a distribution of FI. This variation in FI measurements is attributable to heterogeneity within the microsphere population and the characteristics of the flow cytometer on which the measurements were conducted. Although efforts were made to minimize these effects, they represent an unavoidable aspect of measurements of optical characteristics in large populations by flow cytometry.

The goal of experiments based on dyed microspheres was to demonstrate an experiment-based method whereby an estimate of the dose distribution delivered by a UV reactor could be measured. Since FI is known to also vary with UV dose (see Figs. 4 and 5), it is clear that variations in FI attributable to the dose distribution will also be apparent within a UV-irradiated sample collected from a continuous-flow reactor. Therefore, in the application of this type of method, it is necessary to differentiate variation (error) in FI measurements attributable to the dose distribution from the intrinsic sources of error in measurements of FI by flow cytometry, as well as inherent variations in the physical attributes of the microspheres themselves. Moreover, it is necessary to demonstrate that these sources of error account for the vast majority of variability in these measurements.

For application of this method in estimation of a dose distribution, it was necessary to develop and prove a hypothesis that allows mathematical coupling (and decoupling) of the FI distributions with the dose distribution. It was hypothesized that the FI distribution in a sample containing microspheres that had been subjected to a distribution of doses was attributable to:
1. UV dose distribution;
2. Measurement errors associated with flow cytometry; and
3. Population heterogeneity among the dyed microspheres.
Moreover, it was assumed that these sources of error were independent, and therefore their effects were additive.

In mathematical terms, it was hypothesized that the FI distribution measured in a sample collected from a continuous-flow UV reactor (Fig. 6) could be represented as the convolution of the FI distribution attributable to each individual dose and the dose distribution. To develop this hypothesis further, it was necessary to define the approach used in convolution (and deconvolution), as well as define terms of the convolution (deconvolution) algorithm. For purposes of mathematical analysis, distributions of FI and UV dose were characterized by histograms, with bin widths of 1 FI unit and 1 mJ/cm^2, respectively.

To examine the validity of the convolution hypothesis, an additional experiment was conducted in which subsamples of an aqueous suspension of dyed microspheres were subjected to a range of well-defined, single-valued doses under a collimated beam of monochromatic ($\lambda = 253.7$ nm) radiation in shallow, well-mixed, batch reactors. A total of eight distinct doses were delivered to these samples: 0, 10, 20, 40, 60, 100, 150, and 200 mJ/cm^2. Aliquots from each of these UV exposures were then mixed to provide a suspension that contained equal quantities of microspheres that had been subjected to each of the eight

doses. This method of exposure and mixture allowed development of a (mixed) sample that contained a known dose distribution. Samples from the individual doses as well as the mixed sample were subjected to microsphere preconcentration and analysis by flow cytometry using the methods described previously.

The following definitions were used in analysis of FI responses for microspheres that had been subjected to a well-defined, single-valued UV dose from the collimated-beam experiment: i=index for counting dose (D) increments (bin width=1 mJ/cm^2; $i = 1, 2, \ldots, m$); j=index for counting FI increments (bin width=1 FI unit; $j = 1, 2, \ldots, n$); $C_{j,i}$=number of microspheres that emit FI$_j$ after being subjected to dose D_i; C_i=number of microspheres counted by flow cytometry in sample subjected to $D_i = \sum_{j=0}^{n} C_{j,i}$; $\Gamma_{j,i}$=fraction of particles receiving D_i that emit FI$_j = C_{j,i}/C_i$.

From the definitions listed above, the following identities can be developed:

$$\sum_{j=0}^{n} \Gamma_{j,i} \equiv 1$$

$$\sum_{i,j} \Gamma_{j,i} \equiv m + 1 \qquad (1)$$

For analysis of the mixed sample (i.e., the sample with the known dose distribution), the following definitions were applied: A=total number of FI measurements collected for mixed sample; A_i=number of particles in a mixed sample that receive dose D_i; α_i=fraction of particles in a mixed sample that receive dose $D_i = A_i/A$; B_j=number of particles in mixed sample that emit FI$_j$; and β_j=fraction of particles in mixed sample that emit FI$_j = B_j/A$.

Again, it is possible to develop relevant identities

$$\sum_{i=0}^{m} \alpha_i \equiv 1$$

$$\sum_{j=0}^{n} \beta_j \equiv 1 \qquad (2)$$

In the convolution experiment, the known information from the analysis of the mixed sample by flow cytometry was B_j (or β_j). If the convolution hypothesis is correct, then it should also be possible to calculate the FI distribution in the mixed sample (B_j or β_j) as a linear combination (convolution) of the FI distributions of the individual samples used to develop the mixed sample, and the known fraction of the mixed sample that each individual dose comprised in the mixed sample. In mathematical terms, this may be represented as follows:

$$B_j = \alpha_0 A \Gamma_{j,0} + \alpha_1 A \Gamma_{j,1} + \cdots + \alpha_m A \Gamma_{j,m} = \sum_{i=0}^{m} \alpha_i A \Gamma_{j,i} \qquad (3)$$

or by dividing through by A

$$\beta_j = \sum_{i=0}^{m} \alpha_i \Gamma_{j,i} \qquad (4)$$

Fig. 7 provides a graphical representation of the results of the convolution experiment. The variation in FI at each individual dose is clearly evident in this figure. The results of the convolution are in excellent agreement with the analysis of the mixed
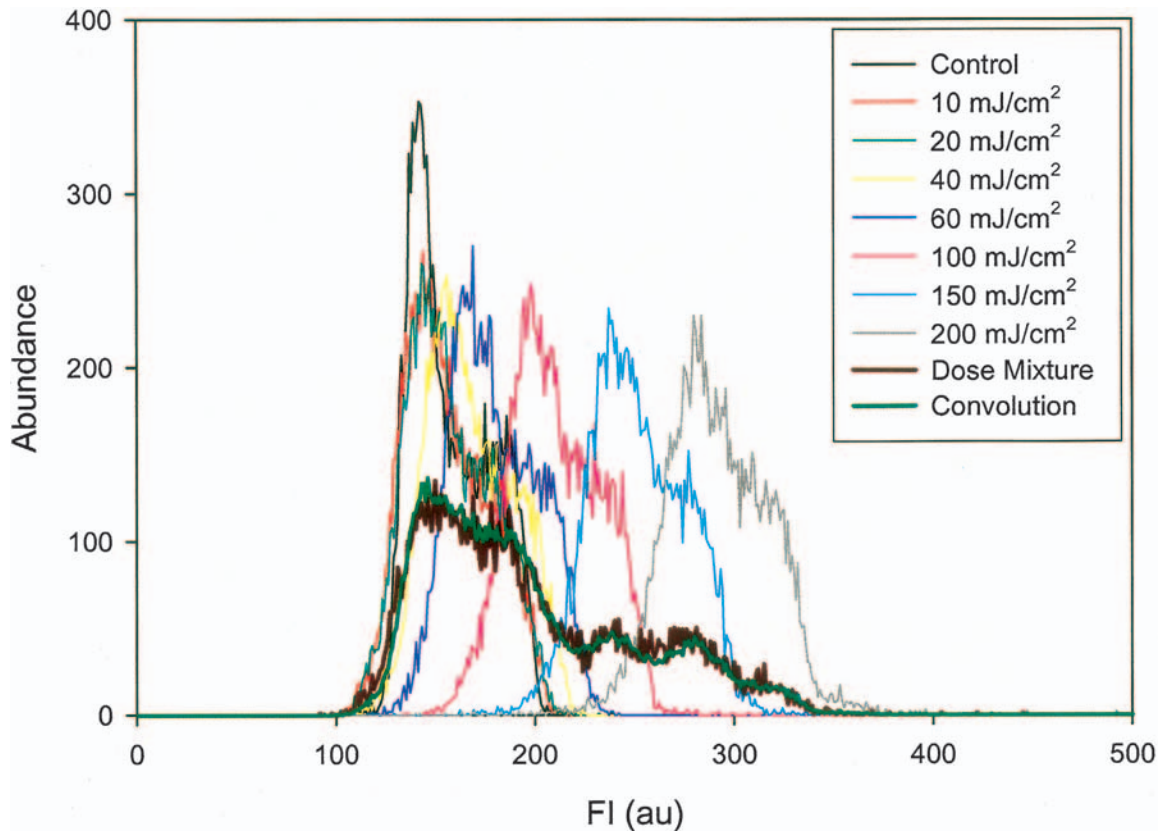
Fig. 7. (Color) Measurements of FI from convolution experiment. FI distributions based on measurements of sample developed from equal-volume mixture of subsamples that had been exposed to known doses under collimated beam (dose mixture) were compared with calculated FI distribution based on convolution of data from individual doses (convolution).

sample ($r^2=0.97$). These data support the validity of the convolution hypothesis.

Deconvolution

The dose–response data from the collimated-beam experiments (Fig. 5) provided detailed information regarding the FI distribution behavior of the dyed microspheres over the range of relevant doses for the reactor system of interest. However, for numerical deconvolution, it was necessary to represent FI distributions among the dyed microspheres (i.e., microsphere dose–response behavior) at a smaller dose interval than was investigated in these experiments. For consistency with the bin width selected for representation of the dose distribution, it was assumed that representation of microsphere dose–response behavior at an increment of 1 mJ/cm^2 would be sufficient for this purpose.

It is impractical to conduct the experiments needed to develop dose–response behavior for dyed microspheres at such a small dose increment for a dose range as wide as is necessary for reactor characterization (0–200 mJ/cm^2). However, the changes in FI distribution along the range of doses 0–200 mJ/cm^2 were quite regular. Therefore, it was assumed that an interpolation scheme could be applied to characterize dose–response behavior in the dose range of interest.

Ideally, an analytical function would be developed to describe the observed changes in FI for the range of doses of interest. No such relationship was identified in this research because the causes of the variation in FI response have not been fully charac-

terized in mathematical terms. Therefore, an empirical approach was used to identify an appropriate interpolation algorithm. Nonlinear regression was used to "fit" the data from Fig. 5 to several well-known density distribution functions. Among these, the Weibull distribution was judged to yield the best fits of the data.

It was noted that a Weibull distribution with location parameter—sometimes referred to as a "three-parameter Weibull distribution"—gave a close fit to the individual FI distributions in Fig. 5. In addition, the three parameters (location, scale, and shape) varied in a convincingly linear fashion over the range of doses. Using regression-fit values of the linear trends, the values of the entries of the matrix Γ were estimated by interpolation.

The mathematical basis of the convolution algorithm was defined in Eqs. (1)–(4). Eq. (4) can be rewritten in matrix notation as

$$[\beta] = [\Gamma] \times [\alpha]$$

where

$$[\beta] = \begin{Bmatrix} \beta_0 \\ \beta_1 \\ \vdots \\ \beta_n \end{Bmatrix}; \quad [\Gamma] = \begin{Bmatrix} \gamma_{0,0} & \gamma_{0,1} & \cdots & \gamma_{0,m} \\ \gamma_{1,0} & \gamma_{1,1} & \cdots & \gamma_{1,m} \\ \vdots & \vdots & \vdots & \vdots \\ \gamma_{n,0} & \gamma_{n,1} & \cdots & \gamma_{n,m} \end{Bmatrix}; \quad [\alpha] = \begin{Bmatrix} \alpha_0 \\ \alpha_1 \\ \vdots \\ \alpha_m \end{Bmatrix}$$

(5)

The objective of deconvolution was to yield an estimate of the dose distribution, which was represented by the vector [α]. For each operating condition, the vector [β] was the FI distribution
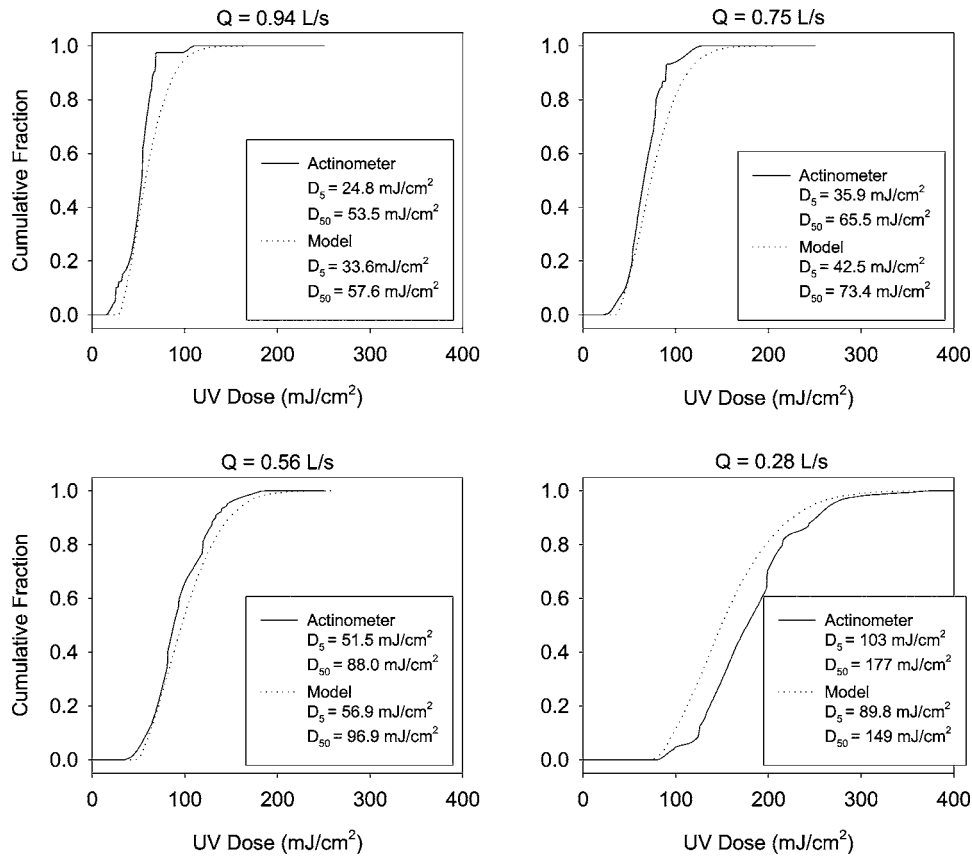
Fig. 8. Estimates of cumulative dose distribution delivered by continuous-flow UV reactor by Lagrangian actinometry and Lagrangian numerical model at four flow rates. Estimates of D_5 and D_{50} are included in legends of figure panels for each method.

(histogram) from the flow cytometry analysis of an effluent sample from the continuous-flow reactor (Fig. 6). The matrix $[\Gamma]$ was developed by application of the interpolation algorithm (using the Weibull distribution) to the data from the flow cytometry analysis of samples exposed under the collimated beam (Fig. 5). The actual deconvolution process was conducted by importing data from the flow cytometry analyses into a MATLAB program, subject to the constraints defined in Eqs. (1)–(3).

Fig. 8 illustrates the deconvolved dose distributions from the experiment with the continuous-flow reactor. Dose distributions are presented in the form of cumulative distribution functions to facilitate comparison with dose distribution estimates based on application of a Lagrangian numerical simulation (discussed in next subsection).

Lagrangian Numerical Model

A numerical simulation of reactor behavior was developed using a component approach. The model was based on the results of simulations accomplished through application of two basic submodels to the reactor system. The first submodel was a numerical representation of the UV irradiance field; the second submodel was a numerical representation of the flow field. The submodels were used to simulate the respective characteristics of the reactor for each of the steady-state operating conditions used in the experiments involving introduction of the dyed microspheres (Lagrangian actinometry) and the *B. subtilis* spores (biodosimetry). The results of these two simulations were linked to develop numerical approximations of the dose distribution corresponding to

each operating condition through a Lagrangian (particle-centered) approach. The resulting dose distribution estimates were linked with the measured dose–response behavior of the challenge organism to yield predictions of *B. subtilis* spore inactivation for each operating condition.

UV Irradiance Field Modeling

The UV irradiance field surrounding a low-pressure mercury lamp was estimated by LSI (Blatchley 1997). The LSI model equation is

$$I(R,z) = \int_0^L \frac{P}{4\pi L_a \rho^2} \exp\left\{ -[\sigma_q t_q + \sigma_w(R - r_q)]\frac{\rho}{R} \right\} dZ \quad (6)$$

where $I(R,z)$=UV irradiance at point (R,z) in the irradiated zone; P=lamp output power; L_a=lamp arc length; L=effective portion of the lamp contributing to irradiance at a point in the reactor; ρ=distance from lamp source to receptor site (R,z); σ_q=absorbance coefficient for the quartz lamp jacket; t_q=thickness of the quartz lamp jacket; σ_w=absorbance coefficient for water; R=radial distance from lamp axis to receptor site; r_q=quartz jacket outside radius; and Z=Cartesian coordinate defining longitudinal distance along the lamp.

The LSI model predicts that for a given radial distance, UV irradiance at the ends of the lamp will be lower than at other axial locations along the length of the lamp. A graphical representation of a simulated irradiance field within the single-lamp reactor is presented in Fig. 9. The conditions of simulation were P=13.4 W, L_a=76.2 cm, L=75.5 cm, σ_q=0.4 cm^{-1}, t_q=1.5 mm, σ_w=0.0062 cm^{-1}, and r_q=1.24 cm. It is important to note that all
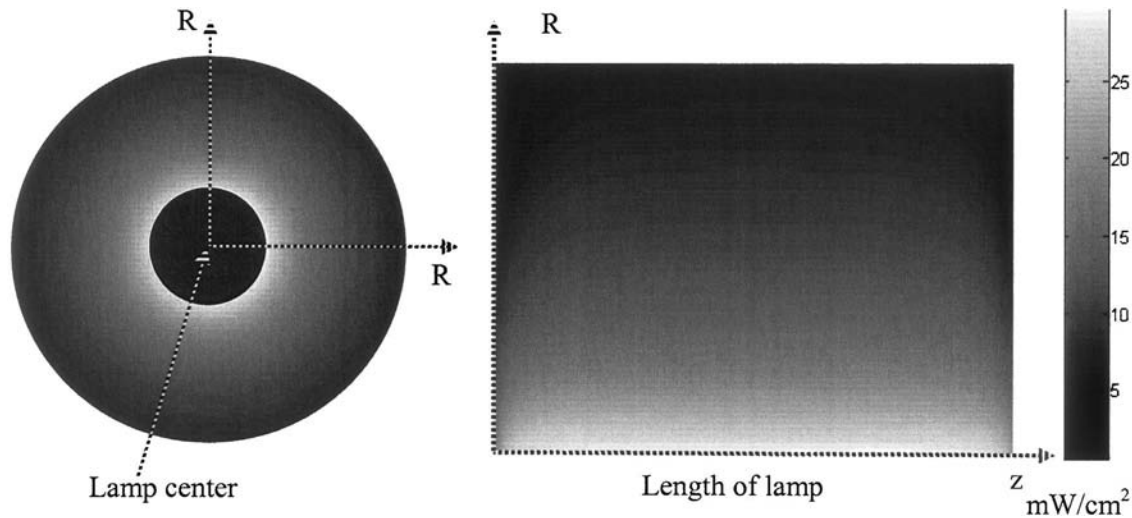
Fig. 9. Radial and longitudinal irradiance profile around single UV lamp

input parameters used in this submodel were based on physical measurements. The lamp output power was calculated from the inverse LSI model (Blatchley 1997) and irradiance readings taken through the reactor viewing port and the flat-plate collimator.

Flow Field and Microbial Trajectory Simulations

Hydrodynamic behavior within the reactor system was simulated using a commercially available CFD package (FLUENT). These simulations were based on a finite-volume approximation to the equations of motion and continuity. Under virtually all operating conditions, photochemical reactors operate in the turbulent regime; the k-ε model was used to accomplish turbulence closure (Launder and Spalding 1972). Mesh generation (tetrahedral elements) was accomplished as a preprocessing operation using GAMBIT (Fluent, Inc.). The computational grid was developed to simulate the closed-chamber, single-lamp UV disinfection reactor described above. As a reminder, the reactor had an internal diameter of 9.55 cm and an internal length of 75.5 cm. The positive z direction was chosen to be parallel to the longitudinal axis of the reactor. An inner, coaxial cylindrical wall was defined to represent the quartz jacket that surrounded the single low-pressure mercury lamp; the cylindrical (quartz) wall had an outside diameter of 2.54 cm. Water flow was confined to the annular region between the lamp (jacket) and the inner wall of the reactor. Also included in the modeled geometry was a viewing port positioned on the wall of the reactor, midway between the entrance and exit ports of the reactor. The viewing port was covered by a quartz window which facilitated measurements of UV irradiance emitted from the lamp. A schematic of this model is presented in Fig. 10, as drawn in GAMBIT.

Based on preliminary flow field solutions, regions of high velocity gradient were identified within the inlet portion of the reactor and close to the outlet. The mesh was refined by employing the size function capability in GAMBIT and additional tetrahedral elements were concentrated in the regions of high gradients. The finer mesh allowed for more accurate resolution of the salient features of the flow field. The resulting three-dimensional mesh was exported into FLUENT. The governing turbulent flow transport equations were solved for each control volume using a second-order discretization scheme. All equations were solved through an iterative procedure to simulate the flow field. The boundary conditions specified were a uniform inlet velocity cal-

culated based on the average flow rate and the diameter of the inlet piping system, zero diffusion flux for all flow variables at the outflow, and a no-slip boundary condition at the solid boundaries (walls of the reactor and lamp jackets). The inlet boundary conditions for k and ε were defined by specifying the turbulence intensity and the hydraulic diameter of the flow upstream of the inlet (*Fluent 6.1 user's guide* 2003). The values for k and ε can be calculated based on these parameters. This was possible as the inlet portion of the reactor that was included in the computational domain was in reality (in the biodosimetry experiments) preceded with 38 cm of straight inlet piping with a diameter of 4.1 cm. The turbulence intensity can be approximated by an empirical correlation for pipe flows based on the Reynolds number (*Fluent 6.1 user's guide* 2003). For the four flow rates used in the biodosimetry experiments, the turbulence intensity was in the range between 4.4 and 5.1%. This procedure was repeated until the flow field solution did not change with further mesh refinement. The refined grid consisted of more than 490,000 tetrahedral control volumes. Convergence of the solution was monitored by examining the scaled residuals after every iteration, which represented the imbalance in the conservation equation for every flow variable
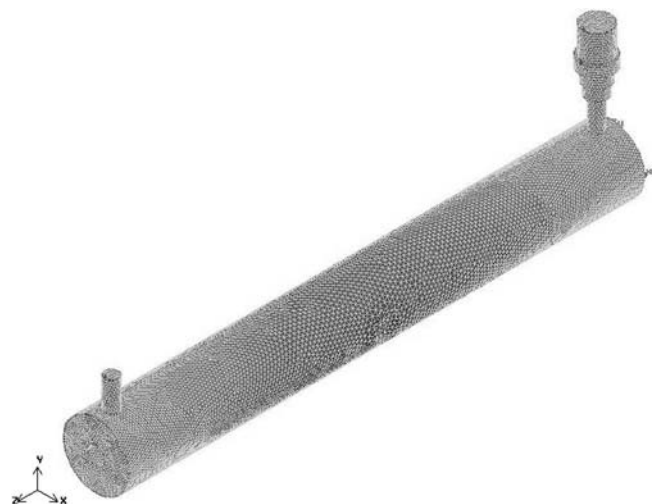

Fig. 10. Closed-vessel UV reactor geometry as modeled in GAMBIT

summed over all the computational cells. Convergence was achieved after approximately 3,000 iterations and when the scaled residuals did not decrease with further iterations. The scaled residuals decreased by five orders of magnitude for the k and ε equations and six orders of magnitude for the continuity and momentum equations.

For each flow condition imposed on the reactor, a solution of the transport equations was developed for the continuous (liquid) phase. FLUENT allows simulation of a discrete second phase using a Lagrangian approach. The particle-tracking algorithm of FLUENT was used to simulate the trajectories of microorganisms and microspheres through the reactor. Particles were modeled as 1.2-μm-diameter spheres of neutral buoyancy. The diameter of the spherical particles was chosen to be representative of the size of *Bacillus subtilis* spores (Nicholson et al. 2000); however, with neutrally buoyant particles in this size range, simulated trajectories are not a strong function of particle size. Therefore, the trajectory simulations developed by the particle-tracking algorithm were also believed to be representative of microsphere trajectories through the reactor.

A target of 10,000 particles was selected as the size of the population of particle trajectories to be simulated for each operating condition. Particle locations were selected to be uniformly distributed across the inlet. To achieve these characteristics, a square section was circumscribed around the circular inlet of the reactor. A 113×113 grid of initial positions (12,769 equally spaced locations) was established across this square section. However, only those positions that existed within the circular cross section of the reactor inlet were included in the simulations. Based on this approach, a population of 10,148 initial particle positions was defined. For each operating condition, a single particle trajectory was simulated from each of these initial positions.

It was assumed that the second phase (particles) was sufficiently diluted to ensure that particle–particle interactions were negligible. The effects of the particle volume fraction on the continuous phase were also assumed to be negligible. Boundary conditions imposed on the discrete phase were a perfect reflection via an elastic collision ("ricochet") from all solid boundaries and an "escape" condition at the outlet, where the particles exited the computational domain.

Particle trajectory calculations were based on a force balance on the particle using the local continuous phase conditions as the particle moved through the flow. Integration (in time) of the trajectory equations yielded the velocity of each particle at each point along its trajectory. The integration time step was selected such that the particle trajectory equation was solved every time a particle crossed a control volume boundary. Control volumes ranged in size from roughly 0.1 mm^3 to 0.1 cm^3, and the corresponding integration time step ranged from roughly 10^{-7} to 10^{-1} s.

The turbulent motion of the particles in the flow field was simulated by using a normally distributed random number to represent the instantaneous velocity fluctuations in the trajectory equations

$$u_i = \bar{u}_i + \xi u' \tag{7}$$

where u_i=instantaneous velocity; $\bar{u}_i$=local mean velocity; i=index to represent the coordinate directions (x, y, and z); ξ is randomly selected from a normal distribution with a value between -1 and 1; and $u' = (2k/3)^{1/2}$. This approach implied that the flow in question was characterized by isotropic turbulence. A step-by-step report of instantaneous particle position and velocity

was generated for each particle; subsequent interrogation of these output files was used for prediction of a particle-specific dose.

Dose Distribution Calculations

A code was written in FORTRAN 90/95 to read the step-by-step particle trajectory position report generated by FLUENT and the corresponding UV irradiance field information. The code then associated each instantaneous particle position with the UV irradiance corresponding to that position. As particle positions generally did not coincide with a grid point at which irradiance was calculated, the value of irradiance assigned to each point was estimated from the four closest grid points through bilinear interpolation. The incremental dose associated with each individual step through the irradiation zone was calculated as the product of the local irradiance, $I(R,z)$, and the time step between two consecutive particle positions. The cumulative particle-specific dose was expressed as the sum of all dose increments that the particle was exposed to during its time in the irradiated zone.

Comparison of Dose Distribution Predictions by Lagrangian Methods

Dose distribution estimates by Lagrangian actinometry and Lagrangian numerical modeling were compared using the parameter D_k; k% of particles in a population were estimated to have received a UV dose of D_k or smaller (see Fig. 8). Therefore, D_{50} represents the median of the dose distribution, while only 5% of the population received a UV dose smaller than D_5.

For the lowest flow rate used in these experiments (0.28 L/s), a fairly substantial difference was observed between the dose distribution estimates by Lagrangian actinometry and the Lagrangian numerical model. The median of the estimated dose distribution (D_{50}) by Lagrangian actinometry was roughly 19% higher than the corresponding estimate from the Lagrangian numerical model.

In a photochemical reactor system, the vast majority of unreacted starting material (parent compound) present in an effluent sample will be attributed to the low-dose end of the dose distribution. The presence of parent compound in the effluent is an indication of poor performance on the part of the reactor. The parameter D_5 was chosen as a representation of the low-dose end of the dose distribution. The largest absolute difference between the estimates of D_5 was 13 mJ/cm^2, again for the case of $Q=0.28$ L/s; this difference between the two estimates of D_5 was roughly 14% of the estimate by the Lagrangian numerical model. Estimates of D_{50} and D_5 for the two methods were generally in good agreement for the other operating conditions.

The relatively large discrepancy between the dose distribution estimates by the two methods for the case of $Q=0.28$ L/s is believed to be largely attributable to the lack of dose–response data for the dyed microspheres for doses above 200 mJ/cm^2; the numerical simulation (which was conducted after the experiments) suggested that a substantial fraction of the microsphere population received doses above 200 mJ/cm^2 at this flow rate. At this low flow rate, extrapolation of measured dose–response behavior was required to estimate the behavior of the microspheres for doses greater than 200 mJ/cm^2; for all other flow conditions, microsphere dose–response behavior was estimated by interpolation. Accurate a priori estimation of the maximum dose to be delivered by a reactor under a given set of operating conditions is difficult. Experiments with the collimated-beam system were limited to doses below 200 mJ/cm^2 because this dose is well beyond reported values of dose used in most operational UV disinfection
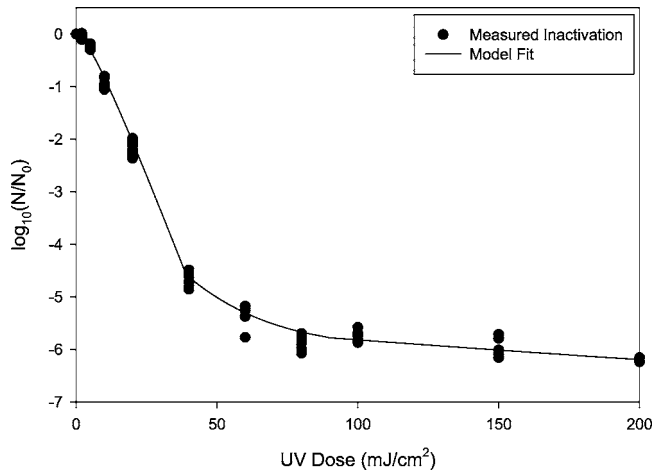
Fig. 11. UV dose–response behavior of *B. subtilis* spores. Irradiation was accomplished in shallow, well-mixed, batch reactors under collimated beam. Model fit from Eq. (8) is also illustrated.

Fig. 12. Comparison of measured *B. subtilis* spore inactivation with predictions from dose distribution estimates from Lagrangian numerical simulation and Lagrangian actinometry

systems, which were the immediate target of this application. However, few reports of dose delivery in these systems have considered the entire dose distribution. This analysis suggests that some photochemical reactors may yield dose distributions that extend well beyond the range of doses normally considered in reactor modeling and validation, at least in the limit of low flow rate and high transmittance.

While general agreement between these two methods of dose distribution estimation is desirable, no standard exists for validation of these estimates. At present, Lagrangian actinometry and numerical modeling represent the only two methods for estimation of a UV dose distribution in a continuous-flow photochemical reactor. Therefore, agreement in dose distribution estimates between Lagrangian actinometry and a Lagrangian numerical model does not represent mutual validation of these methods.

Biodosimetry Experiment: Comparison of Microbial Inactivation Measurements and Predictions

When properly combined with the intrinsic kinetics (i.e., UV dose–response behavior) of inactivation for the challenge organism, an accurate estimation of the dose distribution should yield an accurate prediction of challenge organism inactivation in biodosimetry experiments. Therefore, a key aspect of the biodosimetry experiments was the measurement of the dose–response behavior of the challenge organism.

Fig. 11 provides an illustration of the observed dose–response behavior for the *B. subtilis* spores used in this research. As is typical of this organism, the spores displayed a lag (or shoulder) in the limit of low doses, followed by roughly first-order inactivation, followed by tailing. Fig. 11 describes dose–response behavior for *B. subtilis* spores for a wider range of doses than is normally examined. Representation of this broad dose range was necessary because of the anticipated breadth of the dose distributions.

The series-event model (Severin et al. 1983) was fit to the data for doses ranging from 0 to 40 mJ/cm². Nonlinear regression was used to fit observed inactivation responses in this dose range, resulting in series-event parameter estimates of $n=2$ and $k=0.34$ cm²/mJ. Beyond this dose range, the spores displayed tailing behavior, which is not accounted for by the series-event
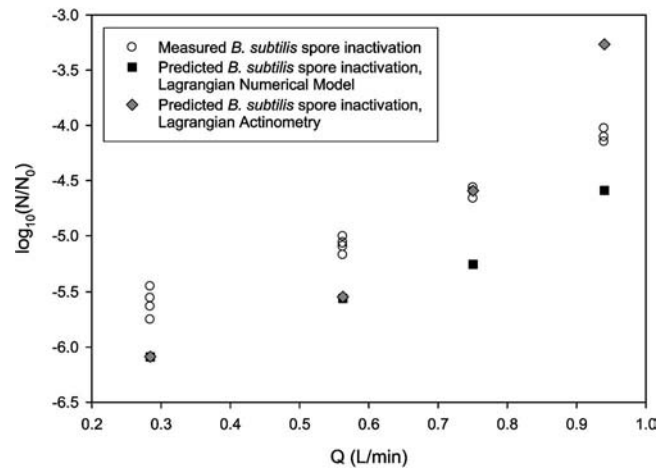
model. Because existing models of UV dose–response behavior do not adequately account for tailing, empirical expressions were used to describe spore dose–response behavior for doses above 40 mJ/cm². For doses ranging from 40 to 90 mJ/cm², a polynomial expression was applied. Inactivation responses for doses above this range were described using a quadratic expression (EPA 2003). Collectively, these three functions [Eq. (8), Fig. 11] were used to represent dose–response behavior of the *B. subtilis* spores

$$D \in (0,40): \frac{N}{N_0} = (1 + 0.34 \cdot D) \cdot \exp(-0.34 \cdot D)$$

$$D \in [40,90): \log\left(\frac{N}{N_0}\right) = 5 \cdot 10^{-9} \cdot D^4 + 4 \cdot 10^{-6} \cdot D^3 + 10^{-3} \cdot D^2$$

$$- 0.1 \cdot D - 1.7 \tag{8}$$

$$D \geqslant 90: D = 40 \cdot \log\left(\frac{N}{N_0}\right)^2 + 216 \cdot \log\left(\frac{N}{N_0}\right)$$

Predictions of challenge organism (*B. subtilis* spores, in this case) inactivation in a continuous-flow reactor (e.g., in the biodosimetry experiment) can be made by integration of an estimate of the dose distribution with measured dose–response behavior for the challenge organism using a mathematical analog of the segregated-flow model (Chiu et al. 1999)

$$\frac{N}{N_0} = \int_0^\infty K_d(D) \cdot E(D) \cdot d(D) \tag{9}$$

where N=concentration of viable challenge organisms in an effluent sample (cfu/mL); N_0=concentration of viable challenge organisms in influent (cfu/mL); $K_d(D)$=UV dose–response behavior of target organism; and $E(D)$=dose distribution function (cm²/mJ).

For each of the operating conditions of the experiment with the continuous-flow reactor, estimates of $E(D)$ were developed by Lagrangian actinometry and the Lagrangian numerical model (see Fig. 8). Therefore, for each case it was possible to develop separate estimates of microbial inactivation by these two methods, and compare these estimates with measurements of challenge organ-

ism inactivation. A summary of these predictions and the measured inactivation responses from the biodosimetry experiments is presented in Fig. 12.

Predicted inactivation responses of the challenge organism were in good agreement with measurements. The largest differences between the predictions by Lagrangian actinometry and measured inactivation responses occurred at the extreme flow rate conditions. However, in all cases, predictions of microbial inactivation were within less than 1 $\log_{10}$ unit of measurements.

The data presented in Fig. 12 for the highest and lowest flow rate conditions used in these experiments illustrate some important features of this method of reactor analysis. Despite the differences between dose distribution estimates by the two Lagrangian methods for the lowest flow rate condition ($Q=0.28$ L/s), good agreement was observed between the predictions of Lagrangian actinometry, the Lagrangian numerical model, and the biodosimetry experiment measurements. However, both Lagrangian methods indicate that the vast majority of particles will receive a dose above 70 mJ/cm^2, which is well into the tailing region of the dose–response curve. Therefore, predictions of *B. subtilis* spore inactivation for this reactor are relatively insensitive to operating conditions in the limit of low flow conditions. Alternatively, it is evident that predictions of reactor behavior in this region are not sensitive to estimates of the dose distribution.

By contrast, predictions of reactor performance (as defined by *B. subtilis* spore inactivation) in the limit of high flow rate were highly sensitive to the dose distribution estimate because a large fraction of the exposed particles were subjected to doses in the range where the dose–response relationship (Fig. 11) is steep. For the case of the highest flow rate condition in these experiments ($Q=0.94$ L/s), dose distribution estimates by the two Lagrangian methods appeared to be in good agreement; yet, the prediction of process performance (i.e., *B. subtilis* spore inactivation through the continuous-flow reactor) resulting from Lagrangian actinometry for this condition was furthest from the prediction by the Lagrangian model and experimental measurements of all the data illustrated in Fig. 12.

Conclusions

Lagrangian actinometry represents an experimental method by which dose delivery in a continuous-flow photochemical reactor system can be measured. This new tool can be used to validate numerical simulations of photochemical reactor performance. More generally, Lagrangian actinometry can be used to develop a comprehensive representation of dose delivery in a photochemical reactor system, accounting for the complex, three-dimensional characteristics of the system, including strong gradients in irradiance and the turbulence characteristics of the flow field.

The combined application of Lagrangian actinometry, numerical modeling, and conventional biodosimetry represents a robust, comprehensive method of reactor assessment. This three-pronged approach provides more detailed information about reactor characteristics and behavior than can be developed by application of any of the methods alone. Moreover, these three methods are complementary, in the sense that they each provide information that can be used to confirm or validate aspects of the other methods of reactor characterization.

References

Bergstrom, D. E., Inoue, H., and Reddy, P. A. (1982). "Pyrido[2,3-d]pyrimidine nucleosides, synthesis via cyclization of C-5-substituted cytidines." *J. Org. Chem.*, 47(11), 2174–2178.

Blatchley, E. R., III. (1997). "Numerical modelling of UV intensity: Application to collimated beam reactors and continuous-flow systems." *Water Res.*, 31(9), 2205–2218.

Chiu, K., Lyn, D. A., Savoye, P., and Blatchley, E. R., III. (1999). "An integrated UV disinfection model based on particle tracking." *J. Environ. Eng.*, 125(1), 7–16.

Demas, J. N., Bowman, W. D., Zalewski, E. F., and Velapoldi, R. A. (1981). "Determination of the quantum yield of the ferrioxalate actinometer with electrically calibrated radiometers." *J. Phys. Chem.*, 85(19), 2766–2771.

EPAU. (2003). *Ultraviolet disinfection guidance manual, draft*, Office of Water, Washington, D.C.

Fang, S., Guan, Y., Blatchley, E. R., III, Lin, L. S., Shen, C., and Bergstrom, D. E. (2003). "Development of a nucleoside analog UV light sensor." *Nucleosides, Nucleotides, & Nucleic Acids*, 22(5–8), 703–705.

Fluent users guide. (2003). Fluent Inc., Lebanon, N.H.

Harris, G. D., Adams, V. D., Moore, W. M., and Sorensen, D. L. (1987). "Potassium ferrioxalate as chemical actinometer in ultraviolet reactors." *J. Environ. Eng.*, 113(3), 612–627.

Hatchard, C. G., and Parker, C. A. (1956). "A new sensitive chemical actinometer. II. Potassium ferrioxalate as a standard chemical actinometer." *Proc. R. Soc. London, Ser. A*, 235(1203), 518–536.

Kuhn, H. J., Braslavsky, S. E., and Schmidt, R. (1989). "Chemical actinometry." *Pure Appl. Chem.*, 61(2), 187–210.

Launder, B. E., and Spalding, D. B. (1972). *Lectures in the mathematical models of turbulence*, Academic, London.

Linden, K. G., and Darby, J. L. (1997). "Estimating effective germicidal dose from medium pressure UV lamps." *J. Environ. Eng.*, 123(11), 1142–1149.

Lyn, D. A., and Blatchley, E. R., III. (2005). "Numerical computational fluid dynamics-based models of ultraviolet disinfection channels." *J. Environ. Eng.*, 131(6), 838–849.

Lyn, D. A., Chiu, K., and Blatchley, E. R., III. (1999). "Numerical modeling of flow and disinfection in UV disinfection channels." *J. Environ. Eng.*, 125(1), 17–26.

Mark, G., Schuchmann, M. N., Schuchmann, H. P., and von Sonntag, C. (1990a). "A chemical actinometer for use in connection with UV treatment in drinking-water processing." *Aqua*, 39(5), 309–313.

Mark, G., Schuchmann, M. N., Schuchmann, H. P., and von Sonntag, C. (1990b). "The photolysis of potassium peroxodisulphate in aqueous solution in the presence of tert-butanol: A simple actinometer for 254 nm radiation." *J. Photochem. Photobiol., A*, 55(2), 157–168.

Nicholson, W. L., Munakata, N., Horneck, G., Melosh, H. J., and Setlow, P. (2000). "Resistance of bacillus endospores to extreme terrestrial and extraterrestrial environments." *Microbiol. Mol. Biol. Rev.*, 64(3), 548–572.

Rahn, R. O. (1993). "Use of potassium iodide as a chemical actinometer." *Photochem. Photobiol.*, 58(6), 874–880.

Rahn, R. O. (1997). "Potassium iodide as a chemical actinometer for 254 nm radiation: Use of iodate as an electron scavenger." *Photochem. Photobiol.*, 66(4), 450–455.

Rahn, R. O., Stefan, M. I., Bolton, J. R., Goren, E., Shaw, P.-S., and Lykke, K. R. (2003). "Quantum yield of the iodide-iodate actinometer: Dependence on wavelength and concentration." *Photochem. Photobiol.*, 78(2), 146–152.

Severin, B. F., Suidan, M. T., and Engelbrecht, R. S. (1983). "Kinetic modeling of U.V. disinfection of water." *Water Res.*, 17(11), 1669–1678.

Shen, C., Fang, S., Bergstrom, D. E., and Blatchley, E. R., III. (2005). "(E)-5-[2-(methoxycarbonyl)ethenyl]cytidine as a chemical actinometer for germicidal UV radiation." *Environ. Sci. Technol.*, in press.

Zhang, J.-Y., Boyd, I. W., and Esrom, H. (1997). "UV intensity measurement for a novel 222 nm excimer lamp using chemical actinometer." *Appl. Surf. Sci.*, 109/110, 482–486.